JOURNAL OF GEOPHYSICAL RESEARCH, VOL. 95, NO. D3, PAGES 2177-2185, FEBRUARY 28, 1990

RAIN ESTIMATION FROM SATELLITES: EFFECT OF FINITE FIELD OF VIEW

Long S. Chiu,[1] Gerald R. North,[2] David A. Short,[3] and Alan McConnell[4]

Abstract. Nonuniform rain rates within a field of view (FOV) and a nonlinear rain rate-microwave temperature (R-T) relation lead to a bias in the estimation of areal average rain rate from spaceborne microwave measurements. This bias is estimated from rain rate data collected during the Global Atmospheric Research Program Atlantic Tropical Experiment (GATE) using an R-T relation which is derived from the model results of Wilheit et al. (1977). The bias is about 25% (30%) for a footprint size of 8 km and increases to about 40% (45%) for a footprint size of 40 km for phase I (II) of GATE. In the large FOV limit of 280-km footprint size, the bias is 48% (50%). An experiment was performed in which the biases calculated from phase I were applied to phase II for different rain rate categories. The empirical correction works quite well. An approximate formula which takes account of the effect of spatial inhomogeneity within the FOV and a nonlinear R-T relation is derived. To first order, the two effects multiply to produce the bias. The bias formula is applied to rain field models. For a rain field model where the autocorrelation function is defined by an exponential, the dependence of the bias on the ratio of the FOV size and the e-folding scale is very similar to those calculated from the GATE data. For a Poisson process rain field model the bias formula shows an inverse dependence on the probability of rain. In this context, the lower percent bias for phase I of GATE can be understood in terms of the higher probability of rain during the same period.

1. Introduction

There is a growing awareness of the importance of accurate measurements of global precipitation to the advancement of our knowledge of the dynamics of the oceans and atmosphere. The lack of a surface-based global network points to satellite monitoring as the ultimate mode of observation [Austin and Geotis, 1980]. Techniques available for this remote sensing problem [Arkin, 1979; Barrett and Martin, 1981; Atlas and Thiele, 1981] are mostly based on empirical relations between cloud properties and precipitation. The usefulness of these techniques is hampered by the lack of surface data for calibration.

[1]Applied Research Corporation, Landover, Maryland.

[2]Climate System Research Program, Texas A&M University, College Station.

[3]Goddard Space Flight Center, NASA, Greenbelt, Maryland.

[4]Pixel Analysis, Silver Spring, Maryland.

Paper number 89JD01646.
0148-0227/90/89JD-01646$05.00

For this reason, many have turned to microwave remote sensing methods for estimating rain because the microwave radiation interacts directly with falling hydrometeors [Wilheit et al. 1977]. Over the oceans, a clear indicator of rain rate is the microwave emission at frequencies below about 20 GHz. Figure 1 shows a schematic diagram (idealized here as an exponential) of the relationship between the brightness temperature and the rain rate for a uniformly covered field of view (FOV) for a given columnar height of rain. At the low rain rates, the brightness temperature increases with rainrate due to absorption and reemission of raindrops and saturates at about 15-20 mm/h. The brightness temperature decreases at the higher rain rates (not represented here) as the effect of scattering by hydrometeors takes a more dominant role. Recent calculations show that the effect of scattering may be more important than previously thought [Wu and Weinman, 1984; Kummerow, 1987]. The relation states that when the FOV is filled with a uniform rainrate R, there will be a corresponding microwave brightness temperature, T. We shall refer to the relation as an R-T relation. For example, at 19.3 GHz (the frequency of the electrically scanning microwave radiometer flown on NIMBUS 5, or ESMR 5), the range of variation is about 150 K with instrument noise of a few degrees.

It is worth noting that uniformly filled beams are rare. The notion of uniformly filled beams comes from consideration of one-dimensional models of rainfall, such as that of Wilheit et al., the validity of which relies on the assumption of horizontal homogeneity. Uniformity depends on the sensitivity of measurement and hence implies that

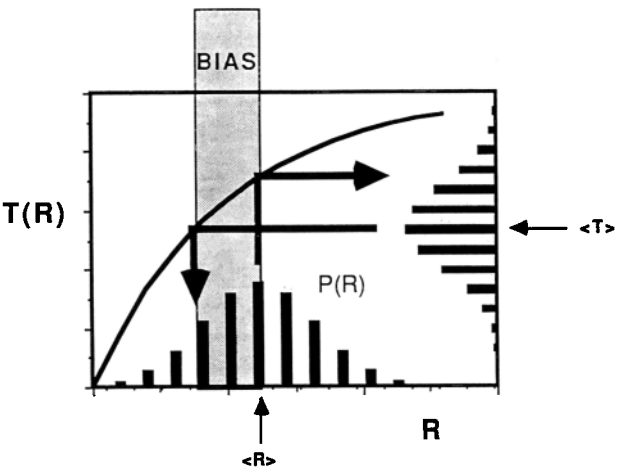

TRANSFORM OF A DISTRIBUTED VARIABLE BY A NONLINEAR FUNCTION LEADING TO BIAS

Fig. 1. Schematic showing the transform of a distribution of rain rate, R, namely, P(R), with mean <R>, through a nonlinear function T(R), where T is the microwave brightness temperature, giving rise to a distribution in T, with mean <T>. The difference between <R> and the rain rate estimated from <T> is called a bias.

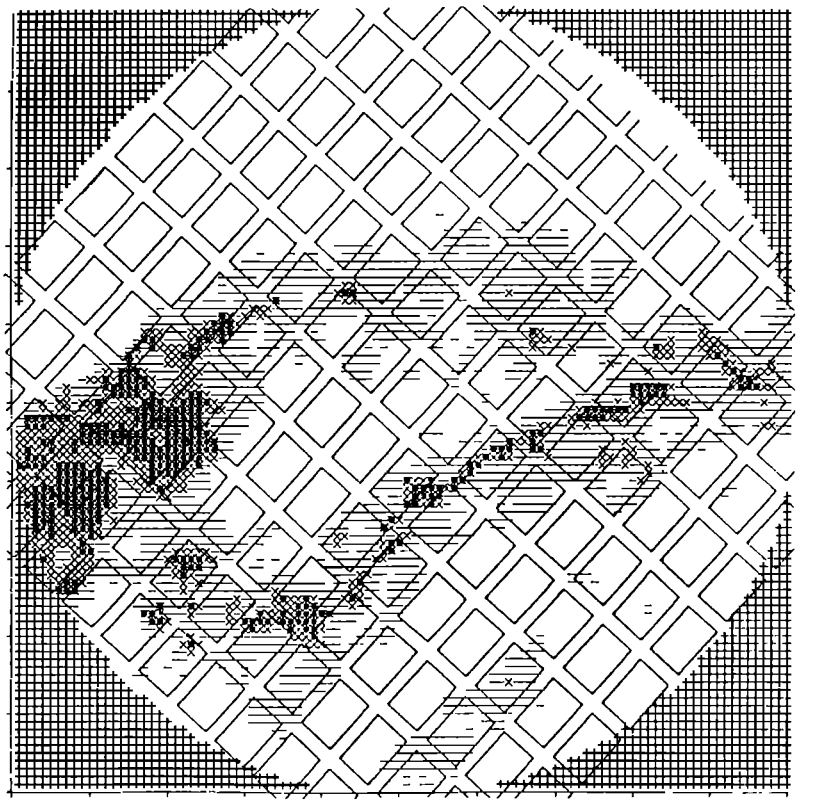

Fig. 2. Schematic showing an instantaneous picture of radar echoes taken during GATE. The shaded and dotted areas show regions of light (>1 mm/h) and heavy (>10 mm/h) rain, respectively. Superposed on it are FOVs of SMMR footprints. Note that the FOVs are rarely uniformly filled.

variations within the beam are less than the accuracy of the sensor.

If all FOVs are filled with uniform rain rates, and in the low rain rate regime where there is a one-to-one correspondence between R and T, the inverse R-T relation can be used to obtain a rain rate for an observed brightness temperature. Although precipitation systems span a wide spectrum, much of the variability is contained in the cumulus scale which is of the order of a few kilometers. Figure 2 shows an instantaneous radar echo pattern observed during the Global Atmospheric Research Program Atlantic Tropical Experiment (GATE) in the Intertropical Convergence Zone (ITCZ) in the Atlantic during the summer of 1974. Overlain is a schematic of the NIMBUS 7 scanning multichannel microwave radiometer (SMMR) 37-GHz channel FOVs. It can be seen that at least in this swath, there are no FOVs which are uniformily filled.

Nonuniform rain rates within an FOV and a nonlinear R-T relation lead to a bias (systematic error) in the estimation of area average rain rate. Within an FOV, rain rates are distributed (see Figure 1). There is an associated distribution of temperature (through the R-T relation). Let square brackets denote areal average over the FOV. The desired quantity is [R], but only [T] is measured. Hence in using the R-T relation, a rain rate of $R_E = R([T])$ is estimated. In general,

$$R([T]) \neq [R]$$

The error incurred in this inversion is

$$\delta R = [R] - R_E$$

A given [R] can give rise to many different R_E because [T] depends on the distribution of R within the FOV.

The ensemble average of δR is called a bias. This bias, often referred to as the "beam filling" bias in remote sensing, has been studied by many investigators [Austin and Geotis, 1978; Smith and Kidder, 1978]. It is, however, worth emphasizing that this bias is not due to unfilled FOVs alone. If the R-T relation is linear, there is no bias associated with the retrieval procedure. The purpose of the paper is twofold. First, the dependence of the bias on resolution is examined using observed data from GATE. Qualitative knowledge of the dependence will be useful in the design of spaceborne precipitation experiments such as the proposed Tropical Rainfall Measuring Mission (TRMM) [Simpson et al., 1988]. Second, simple models are proposed which delineate the effects of a nonlinear R-T relation and unfilled FOVs. It is hoped that experience gained from these models will provide rationale for the removal of the bias associated with rain estimation from microwave observations.

2. Bias Estimates From GATE

2.1. The GATE Data

The radar-derived rain rate data collected during GATE are used. GATE was conducted in the summer of 1974. During roughly three triweekly periods, each termed a phase, extensive radar and

rain gage measurements were made over an area of about 400 km in diameter, called the B-scale area, centered around 8.5°N and 23.5°W. Arkell and Hudlow [1977] composited the radar measurements from research vessels and presented an atlas of the radar reflectivities every 15 min. Patterson et al. [1979] binned the data into 4 km by 4 km pixels and converted the radar reflectivity into rainrates. During phases I and II of GATE, the data were composited mainly from radar measurements collected by the C-band radar on board the research vessel Oceanographer which was positioned at the center of the B-scale. During phase III, Oceanographer was moved to the southeast quadrant. Only data from phases I and II are used in our study.

2.2. Rain Rate-Temperature Relation

The R-T relation used in our study is a functional fit to the model results of Wilheit et al. [1977] for a rain column of 4 km and is of the form

$$T(R) = 274 - 102 \exp(-cR) \quad R < 20 \text{ mm/h} \qquad (1)$$
$$T(R) = 276.44 - 0.22\,R \quad R \geq 20 \text{ mm/h}$$

where T is the brightness temperature in degree Kelvin, R is rain rate in mm/h, and $c = 0.19\ (\text{mm/h})^{-1}$. In this representation we assume that emission is dominant for rain rates less than 20 mm/h and scattering takes over for higher rain rates.

2.3. Bias Calculation

The original data are arranged in an array of 100 by 100 4-km pixels. Sixteen boxes, arranged in 4 by 4 arrays in a checkerboard fashion (Figure 3), are chosen within the whole array. The FOVs chosen for the calculation are situated at the upper left-hand corner of these shaded boxes.

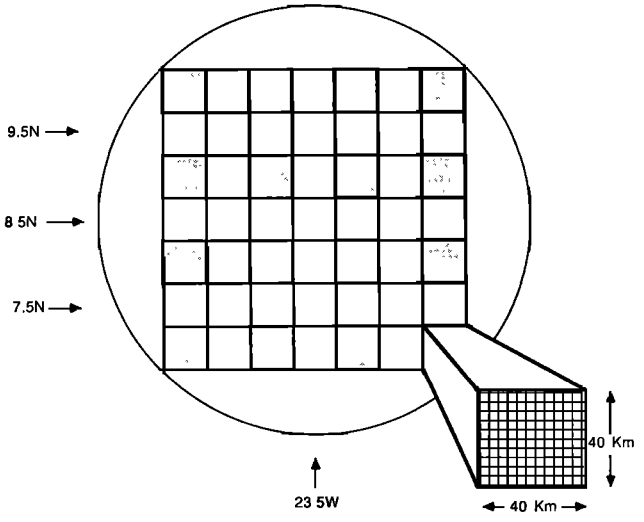

Fig. 3. Schematic of GATE B-scale with 40-km FOVs superposed upon the 4-km bins. The shaded boxes indicate regions where the biases are calculated.

Figure 3 shows the configuration for FOVs of 40 km on a side. This procedure of sampling at regular intervals attempts to minimize the effect of spatial dependence between neighboring boxes of the rainfall data. For different box sizes, the errors are calculated as

$$\delta R = [R] - R([T]) = [R] - R_E$$

where, again, square brackets denote area average over the box (FOV) whose size can be varied. The bias is obtained by ensemble averaging, which is replaced by time averaging, denoted by angle brackets. Biases as functions of the mean rain rates over boxes (FOVs) of side lengths of 8 and 40 km are depicted in Figure 4. The biases are almost linearly related to the mean rain rate in the FOV: linear regression analyses showed correlation coefficients larger than 0.9 which are significant above the 99.5% level. Henceforth, the biases are expressed in terms of the percent of the FOV rain rate, $\langle \delta R \rangle = \alpha \langle [R] \rangle$. The true rainrate can be estimated from R([T]) as

$$\langle [R] \rangle = R(\langle [T] \rangle)/(1 - \alpha)$$

The percent bias is defined as

$$\beta = (\langle [R] \rangle - R_E)/ \langle [R] \rangle$$

The percent bias averaged over the 16 samples for different FOV sizes is presented in Figure 5 for phases I and II. The error bars indicate plus and minus 1 standard deviation calculated from the 16 samples. It can be seen that the percent bias increases from about 25% (30%) for an FOV of 8 km to about 40% (45%) for an FOV of 40 km for phase I (II). These curves suggest an asymptotic limit for large FOVs. The bias for an FOV of 280 km (i.e., taking all data in the large square as shown in Figure 3) is calculated. The bias is 0.223 mm/h (0.185 mm/h) for phase I (II) which has an average rainrate of 0.464 mm/h (0.364 mm/h), and hence a percent bias of 48.1% (50.7%).

2.4. An Experiment

How well can we do if the biases are corrected empirically? We performed an experiment where the biases, sorted according to the "observed" temperature from phase I, were added to the "observed" rain rates in phase II. We then compared these corrected estimates to the true phase II rain rates. This comparison was performed for a variety of FOV sizes, from 2 x 2 (a side length of 8 km) to 10 x 10 (side length of 40 km), 12 x 12 (side length 48 km), and 15 x 15 (side length 60 km).

To compute the biases, we took all possible disjoint adjacent L x L square FOVs from each of the 1716 scans of phase I. The computation has been carried out for L = 2, 3,..., 10, 12, and 15. For each FOV, the true rain rate is

$$[R] = 1/L \times L \sum_{i=1}^{LxL} R_i$$

and the "observed" microwave brightness temperature is

$$[T] = 1/L \times L \sum_{i=1}^{LxL} T(R_i)$$

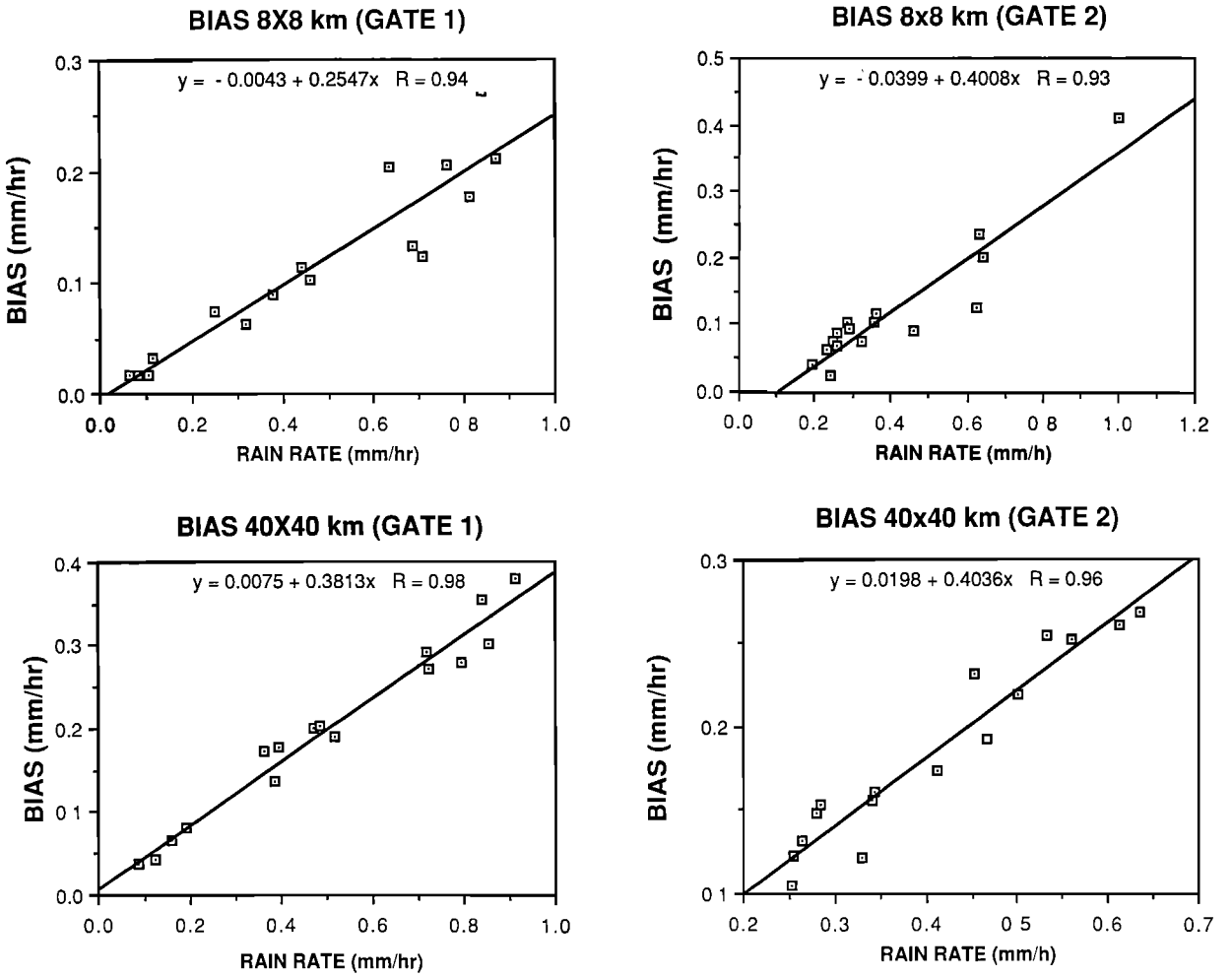

Fig. 4. Scatter diagrams of biases and mean rain rates. The straight lines show linear regression fits to the data.

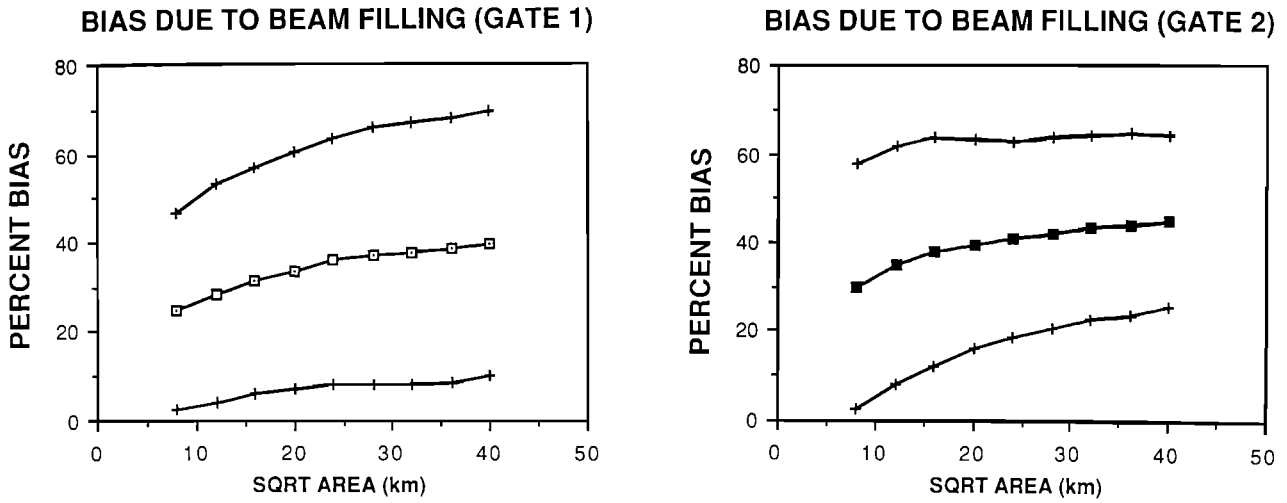

Fig. 5. Calculated bias as a function of the size of FOVs for (left) GATE I and (right) II. The upper and lower curves (represented as pluses) in the figures show the mean ± 1 standard deviation calculated from the 16 samples, respectively. the FOVs are rarely uniformly filled.

We sorted the observed brightness temperatures into 12 categories: six categories below 259 K, corresponding to the low rain rate interval from 0 to 10 mm/hr, where there is a one-to-one correspondence between rain rate and temperature; and six categories above 259 K, corresponding to high rain rates where the R-T relation becomes multivalued. For [T] less than 259 K, we invert the temperature to get a unique corresponding rain rate from the R-T relation. This is the "estimated" rain rate, R_E. For the high rain rate categories, it can be shown that the true rainrates, [R], are bounded by the rain rates corresponding to the observed [T] in the multivalued R-T curve (see Appendix A). For the high rain rate categories, we calculate the statistic

$$\xi = \{[R] - R_A\}/\{R_B - R_A\}$$

where R_A and R_B are the rain rates corresponding to the observed microwave brightness temperature [T], i.e.,

$$T(R_A) = T(R_B) = [T] \qquad R_A < R_B$$

Note that ξ is simply the error introduced if we estimate [R] by R_A, normalized by the difference of the bounds of the rain rate, $R_B - R_A$.

Table 1 displays the biases for FOVs of side length 3 (12 km), 6 (24 km),9 (36 km), and 12 (48 km) pixels. The bias increases with the "observed" rain rate for a fixed FOV and increases with the size of the FOV for each of the first six low rain rate categories. At the high rain rate categories, the ξ increase with the rain rate categories. But it should be remarked that they are less stable, since the number of samples within each category is much less than those at the low rain rate categories. For a side length of 48 km, for example, there is no FOV with a temperature above 268 K (categories 11 and 12).

The rain rate data in phase II are sorted and sampled in a similar manner. The biases derived from phase I (Table 1) are added to the corresponding categories. For categories 7-12, the ξ from Table 1 are added to the ξ calculated from phase II. The corrected ξ are then converted back to rain rate by multiplication by the normalizing factor. Table 2 compares the observed (lower number) and the corrected (upper number) rain rates for each of the 12 categories.

TABLE 1. Bias for FOV sizes of 12, 24, 36, and 48 km Estimated From GATE I

Category	Range	12 km	24 km	36 km	48km
1	0-0.5 mm/h	0.0244	0.0386	0.0455	0.0501
2	0.5-1 mm/h	0.1886	0.3270	0.4232	0.4996
3	1-3 mm/h	0.6041	1.0275	1.2338	1.3277
4	3-5 mm/h	1.3992	2.2428	2.4729	2.6736
5	5-7 mm/h	2.2118	3.1878	3.4854	3.5319
6	7-10 mm/h	3.4707	4.3404	4.5533	4.6067
7	259-262 K	0.0920	0.0833	0.0964	0.1043
8	262-264 K	0.1372	0.1312	0.1145	0.1298
9	264-266 K	0.1952	0.1673	0.1280	0.1336
10	266-268 K	0.2717	0.2351	0.2428	0.3002
11	268-270 K	0.3891	0.3531	0.3309	no data
12	270-273 K	0.5339	0.4830	no data	no data

Table 2. Corrected and True Rain Rates (in mm/h) for GATE II for the Same Rain Rate Categories as in Table 1

Category	Range	12 km	24 km	36 km	48 km
1	0-0.5 mm/h	0.1908	0.1683	0.1608	0.1579
		0.1883	0.1697	0.1636	0.1628
2	0.5-1 mm/h	0.9071	1.038	1.132	1.213
		0.9180	1.096	1.203	1.312
3	1-3 mm/h	2.365	2.744	2.895	2.960
		2.503	3.028	3.202	3.292
4	3-5 mm/h	5.264	6.077	6.273	6.501
		5.886	7.075	7.364	7.994
5	5-7 mm/h	8.099	9.058	9.284	9.238
		9.438	10.632	11.276	10.648
6	7-10mm/h	11.800	12.429	12.815	12.841
		14.025	14.093	14.618	14.686
7	259-262 K	16.300	15.767	16.588	no data
		18.154	18.322	18.020	
8	262-264 K	18.454	18.164	17.323	18.270
		21.117	19.082	19.407	16.555
9	264-266 K	20.392	19.282	17.770	18.078
		23.417	21.010	33.941	17.624
10	266-268 K	21.939	20.869	21.532	no data
		24.006	21.550	15.213	
11	268-270 K	22.939	22.336	21.448	no data
		22.776	24.093	21.217	
12	270-273 K	22.898	22.702	no data	no data
		22.142	21.562		

Inspection of Table 2 shows that discrepancies exist for large FOVs at the high-temperature categories. The extreme case occurs at an FOV of side length 36 km, category 9, which shows a true rain rate of 33.9 mm/h and a corrected rainrate of only 17.8 mm/h. The discrepancies are probably due to sampling. However, the differences between the corrected and true rain rates are in general fairly small. This close match suggests that empirical correction might be a viable approach for the removal of the bias.

3. Theoretical Considerations

3.1. An Approximate Formula

In this section, an approximate formula for the bias is derived which can be considered a rule of thumb for estimating the bias. Consider the function T(R) of the R-T relation as shown in Figure 1. For simplicity, we consider a one-to-one functional between R and T, i.e., no scattering. Let R_E be the estimated rain rate from the measured temperature [T], i.e.,

$$[T] = T(R_E) \qquad (2)$$

A Taylor expansion of T(R) about the area averaged rainrate [R] gives

$$T(R) = T([R]) + (R-[R])T'([R]) + 1/2(R-[R])_2\ T"(R_1) \qquad (3)$$

where R_1 is a value intermediate between R and [R]. If we apply the area- averaging operator (in square brackets) to (2), the linear term vanishes and we obtain

$$[T(R)] = T([R]) + 1/2\ [(R - [R])^2\ T"(R_1)]$$

If T" is continuous, then there exists R_2 such that

$$[(R-[R])^2\ T"(R_1)] = [(R-[R])^2]\ T"(R_2)$$

so that we can write

$$[T(R)] - T([R]) = 1/2[(R-[R])^2]\ T"(R_2) \qquad (4)$$

Note that since T is concave downward (Figure 1), the right-hand side of (4) is negative; thus the (area average of the) instrumental signal is always less than (T of) the true rain rate. Applying the mean-value theorem, we can write

$$T(R) = T([R]) + (R-[R])T'(R_3)$$

for some R_3 between R and [R]. In particular, if the above equation is evaluated at $R = R_E$, we get

$$[T(R)] - T([R]) = (R_E-[R])T'(R_3) \qquad (5)$$

Equating the right-hand sides of (4) and (5), we obtain

$$[R] - R_E = -1/2\ [(R - [R])^2]T"(R_2)/T'(R_3) \qquad (6)$$

Equation (6) expresses an exact relation of the error in the retrieval in terms of the variance of the rain field and the R-T relation. The terms involving R_2 and R_3 are difficult to evaluate. With a possible loss of mathematical precision, compensated for by a gain in elegance and expressiveness, we can write

$$\delta R = [R] - R_E \approx -1/2[(R-[R])^2\ T"([R])/T'([R])] \qquad (7)$$

Taking ensemble averages of (7) gives us the bias. The formula (7) shows that the bias is neatly factored into two parts. The first is a property of the rain field only, namely, the variance with respect to the averaging area (the mean square deviation from the areal mean over the FOV). The second is dependent only on the R-T relation. This formula is consistent with our earlier notion that the error is due to nonuniform rain rate over the FOV and a nonlinear R-T relation. It is intuitively pleasing to see that to first order the two effects multiply to produce the bias.

The sign of the bias can also be estimated to first order from the formula. The first factor (variance) is always positive and depends on the variability of rain rates in the rain field. The second term depends on the ratio of the curvature and the slope of the T(R) curve of the R-T relation. The term T"/T' = -c is negative. Hence a positive bias is anticipated in the retrieval of rain rates from ESMR 5: R_E underestimates [R] in most cases. This is consistent with our results in section 2 and those of previous investigators.

The formula indicates that the error is dependent on the rainrate variance within the FOV. This can be tested by using the GATE data. If we take the logarithm of both sides of (7), we get

$$\log \delta R \approx \log [(R - [R])^2] + \log T"/2T'$$

From the GATE data, the logarithm of the rain rate variance explains about 80% of the variance of the logarithm of the error. The histograms of log [R], log δR, and log $[(R - [R])^2]$ for a 40-km FOV have been calculated (not shown). When plotted on a logarithmic scale, they all show a bell-shaped distribution, suggesting that they are lognormally distributed. We next apply (6) to some simple models of rain fields and examine the associated biases.

3.2. Poisson Process Model

Consider subdividing the FOV into N square tiles. Let x of the N tiles be raining with rain rate r_0 and in the rest of the N - x tiles, there is no rain. Let the probability of rain in an individual tile be p. If p is small and the probability of rain in one tile is independent of the other, we may adopt a Poisson model of the rain field. For a given realization of the process, the area average rain rate in the FOV is

$$[R] = x\ r_0/N$$

and

$$[R^2] = x\ r_0^2/N$$

Taking ensemble averages and using the properties of Poisson statistics, we find that the percent bias is

$$\beta = -\ r_0(1 - p - 1/N\ )T"/2T' \qquad (8)$$

From analysis of GATE data, the average rain rate conditional on positive rain rates for 4-km pixels is about 4 mm/h and the p are 12% and 9% for phase I and II, respectively [Chiu, 1988]. Since β depends on (1 - p), all other parameters being the same, the percent bias should be larger in phase II than in phase I, since p is larger for phase I, which is consistent with Figure 5. In the limit as $N \to \infty$ and $p \to 0$, which corresponds to the large FOV case, the percent bias becomes

$$\beta = r_0c/2$$

if we use the same model of T(R) (equation (1)) adopted in section 2. Putting in numerical values, β is about 40%. The model can be generalized to the case of multiple rain rate categories. Very similar results are obtained.

3.3. Rain Field With a Length Scale

The bias formula can be expressed as a high-pass filter of the spatial spectrum. The case of a one- dimensional rain field is derived in Appendix B. Consider the case where a length scale exists in the rain field, the

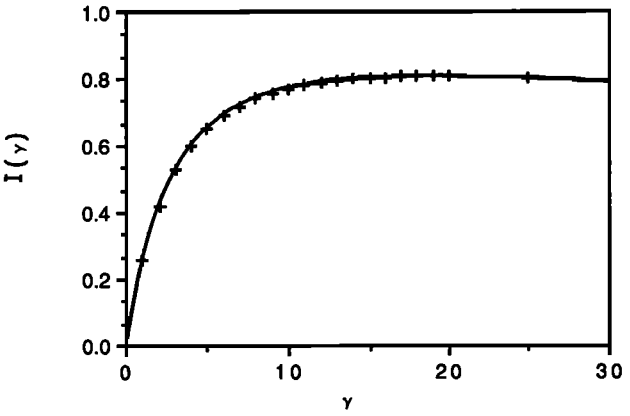

Fig. 6. I(γ) versus γ, where γ is the ratio of the size of the FOV to the length scale in the one-dimensional rain field.

autocorrelation function can be represented as

$$\rho(\underline{s}) = \exp(-|\underline{s}|/\lambda)$$

where $\underline{s}$ is the separation. The normalized spectrum is

$$S(\upsilon) = 2/\lambda\ [1/\lambda^2 + (2\pi\ \upsilon)^2]^{-1}$$

where υ is the wave number or the inverse of the wavelength. If we substitute the spectrum into (B1) in Appendix B, we get

$$\langle \delta R \rangle = T''/2T'\ \sigma^2\ I(\gamma)$$

where I(γ) is the integral

$$I(\gamma) = 2/\pi \int_{-\infty}^{\infty} \gamma/[\gamma^2+(2x)^2]\ [1 - G^2(x)]\ dx$$

$G^2(x)$ is the Bartlett filter given in Appendix B and $\gamma = a/\lambda$ is the ratio of the size of FOV of the sensor to the length scale of the rain field. Figure 6 shows the integral I(γ) as a function of γ. For $\gamma \to 0$, $I(\gamma) \to 0$, which is the case when the FOV is small compared with the length scale of the rain field, and we expect the beam filling error to be minimal. The integral increases to a maximum of about 0.8 for $\gamma = 20$ and decreases slowly as γ increases. As $\gamma \to \infty$, $I \to 0$. The ratio of I(γ=4) to I(γ=20) is about 0.75 which may be compared with the ratio of the biases for FOVs of 8 to 40 km (Figure 5). In the limit when $a >> \lambda$; $I(\gamma) \to 0$. It seems that the formula breaks down in the large FOV limit in the one dimensional case.

4. Summary and Discussion

The bias associated with nonuniformly filled FOVs of spaceborne microwave sensors has been estimated from radar data collected during GATE. An approximate formula is derived which shows that this bias is closely related to the variance of rain rate within the FOV of the sensor. By applying simple models of rain field to the formula, we show that the formula is consistent with variation of the bias.

For the case of a one-dimensional rain field with a decorrelation scale, our calculations show that the bias saturates for $\gamma \approx 10$. If this is compared with Figure 5, which shows a tendency to saturation at a FOV of about 40 km, we may infer a length scale of the rain field of about a few kilometers, for an ESMR 5 FOV which is typically 30-40 km. A note of caution here: the biases we presented in Figure 5 are based on statistics on 4-km pixels, and hence the term which involves the variance of point rainfall (i.e., $[(R - [R])^2]$) may be underestimated. A better estimate may be obtained by resorting to high-resolution radar data (1 km) or data from dense rain gage networks.

Our formula also breaks down in the large FOV limit, probably due to the neglect of higher order terms in the expansion. Short [1988] proposed a statistical model in examining the ESMR 5 data for rainfall retrieval. In his model, the whole ensemble of rain rates is transformed and hence can be compared with the large FOV limit in our case. He showed that rain rate inferred from the microwave brightness temperature underestimates the true rainrate by a factor which depends on the mean and variance of the rainrate distribution, a result which supports our formula.

Much of the preceding is predicated on the assumption that a horizontal length scale exists for rain fields. This assumption has recently been questioned and the notion of fractals in rain rate process has been introduced [Lovejoy and Mandelbrot, 1985; Lovejoy and Schertzer, 1985]. Analyses of rain gage data, however, show no evidence of scaling for rainrate increments in time [Zawadzki, 1987]. Kedem and Chiu [1987] argued that due to the intermittent nature of rain fields, they cannot be self-similar in a strict sense. It appears that in the satellite retrieval case, the question of self-similarity down to essentially infinitesimal scales is avoided by the fact that the microwave temperatures are results of integrating vertically through the column of rain. In other words, a length scale (the height of rain column) is naturally imposed in the retrieval problem.

We showed that the bias associated with nonuniformly filled FOVs of microwave sensors is large but can be corrected. This bias depends strongly on the rain rate variance over the FOVs. This term needs to be estimated globally if the formulation is to be adopted in algorithms of satellite rainfall retrieval. By invoking Taylor's frozen field hypothesis, the equivalence of time and area averages has been demonstrated in some cases [Zawadzki, 1975]. Data from the global network of rain gages can be used to estimate the rain rate variance term. Rain field models are also needed to enhance our understanding of the physics of the bias associated with nonuniformly filled FOVs of microwave sensors.

Appendix A: Boundedness Of The True Rain Rate [R]

We show here that if the R-T relation is multivalued, the true rain rate is bounded. Consider the region where the R-T relation becomes multivalued. Let the rain rates in the R-T relation corresponding to [T] be R_A and R_B, respectively, $R_A \leq R_B$, i.e., $[T] = T(R_A) = T(R_B)$. We will show that if [R] is not in the interval $[R_A, R_B]$, then T([R]) would be less than [T]. This can be seen graphically by examining the R-T relation given by (1) in section 2.2. (T is concave downward and its maximum is located inside

the interval $[R_A, R_B]$.) The fact that $T([R]) < [T]$, however, contradicts results in (4) in section 3.1 , which states that

$$[T] < T([R]) \quad \text{for } R > 0$$

for negative curvatures in the R-T relation. Hence given

$$T(R_A) = T(R_B) = [T]$$

then

$$R_A \leq [R] \leq R_B$$

which is the desired result.

Appendix B: Spectral Representation Of The Bias Formula

We consider the Fourier representation of a one-dimensional rain field following notations used by North and Nakamoto [1988]

$$R(x) = \int_{-\infty}^{\infty} \exp(i2\pi\nu x) R_\nu \, d\nu$$

where

$$R_\nu = \int_{-\infty}^{\infty} \exp(-i2\pi\nu x) R(x) \, dx$$

and ν is the wave number and equals $1/\lambda$, where λ is the wavelength. Assuming an FOV of size a, the area-averaged rain rate is

$$[R] = 1/a \int_{-a/2}^{a/2} dx \int_{-\infty}^{\infty} \exp(i2\pi\nu x) R(\nu) \, d\nu$$

$$= \int_{-\infty}^{\infty} R_\nu \, (\sin \pi\nu a)/\pi\nu a \, d\nu$$

$$= \int_{-\infty}^{\infty} R_\nu \, G(\pi\nu a) \, d\nu$$

where $G(x) = \sin(x)/x$ is the familiar sinc function in physical optics [Hecht and Zajac, 1974] the square of which is also known as the Bartlett filter in time series analysis [Blackman and Tukey, 1959]. Using the orthogonal relation for homogeneous statistics

$$\langle R_\nu R_{\nu'} \rangle = \sigma^2 \delta(\nu - \nu') S(\nu)$$

where δ denotes the Dirac delta function and is zero except at $\nu = \nu'$, σ^2 is the point variance, and $S(\nu)$ is the wave number spectral density, it can be shown that

$$\langle [R]^2 \rangle = \sigma^2 \int_{-\infty}^{\infty} G(\pi\nu a)^2 \, S(\nu) \, d\nu$$

and

$$\langle [R^2] \rangle = \sigma^2 \int_{-\infty}^{\infty} S(\nu) \, d\nu$$

Hence

$$\langle [(R-[R])^2] \rangle = \sigma^2 \int_{-\infty}^{\infty} S(\nu) \, [1 - G(\pi\nu a)^2] \, d\nu \quad \text{(B1)}$$

The term in brackets on the right hand side acts like a high- pass filter on the spatial spectrum R_ν. Hence if the spatial spectrum of rain is known, the bias formula can be readily evaluated.

Acknowledgments. This work is supported in part by the National Aeronautics and Space Administration through grants NAG-5-869 and NAS5-30083.

References

Arkell, R., and M. Hudlow, GATE International Meteorological Radar Atlas, US Government Printing Office, Washington, D. C., 1977.

Arkin, P. A., The relationship between fractional coverage of high cloud and rainfall accumulation during GATE over the B-scale array, Mon. Weather. Rev., 107, 1382-1387, 1979.

Atlas, D., and O. Thiele, Precipitation measurements from space, workshop report, NASA, Goddard Space Flight Center, Greenbelt, Md., Oct., 1881.

Austin, P., and S. Geotis, Evaluation of the quality of precipitation data from a satellite-borne radiometer, NASA report under grant NSG-5024, Mass. Inst. of Tech., Cambridge, 1978.

Austin, P., and S. Geotis, Precipitation measurements over the oceans, in Air Sea Interaction, edited by F. Dobson, L. Hesse, and R. Davis, Plenum, New York, 1980.

Barrett, E. C., and D. M. Martin, The Use of Satellite Data in Rainfall Monitoring, 340pp, Academic, New York, 1981.

Blackman, R. B., and J. W. Tukey, 1959: The Measurement of Power Spectra, 190 pp, Dover, New York, 1959.

Chiu, L. S., Estimating areal rainfall from rain area, in Tropical Precipitation Measurements, edited by J. Theon and N. Fugono, pp. 361-367, Deepak, Hampton, Va., 1988.

Hecht, E., and A. Zajac, Optics, 565 pp., Addison-Wesley, Mass., 1974.

Kedem, B., and L. Chiu, Are rainrate processes self-similar? Water Resour. Res., 23, 1816-1818, 1987.

Kummerow, C., Microwave radiances from horizontally finite, vertically structured precipitating clouds, Ph.D. Dissertation, Univ. of Minn., Minneaplis, 1987.

Lovejoy, S., and B. Mandelbrot, Fractal propreties of rain and a fractal model, Tellus, 37A, 209-232, 1985.

Lovejoy, S., and D. Schertzer, Generalized scale invariance in the atmosphere and fractal models of rain, Water. Resour. Res., 21, 1233-1250, 1985.

North, G., and S. Nakamoto, Formalism for comparing rain estimation designs, paper presented at the Conf. on Mesoscale Precipitation: Analysis, Simulation and Forecasting, AGU/ Amer. Meteor. Soc., Dedham, Mass., Sept. 13-17, 1988.

Patterson, V. L., M. D. Hudlow, P. J. Pytlowany, F. P. Richardson, and J. D. Hoff, GATE radar rainfall processing system, NOAA Tech. Memo., EDIS 26, 1979.

Short, D. A., A statistical-physical interpretation of ESMR-5 brightness temperatures over the GATE area, in Tropical

Precipitation Measurements, edited by J. Theon and N. Fugono, pp. 201-206, Deepak, Hampton, Va., 1988.

Simpson, J., R. F. Adler, and G. R. North, A proposed Tropical Rainfall Measuring Mission (TRMM) satellite, Bull. Am. Meteorol. Soc., 69(3), 278-295, 1988.

Smith, E. A., and S. Q. Kidder, A multispectral satellite approach to rainfall estimates, 26 pp. plus tables and figures, Colo. State Univ., Fort Collins, 1978.

Wilheit, T. T., A. T. C. Chang, M. S. V. Rao, E. B. Rodgers and J. S. Theon, A aatellite technique for quantitatively mapping rainfall rates over the oceans, J. Appl. Meteorol., 16, 551-560, 1977.

Wu, R., and J.A. Weinman, Microwave radiances from precipitating clouds containing aspherical ice, combined phase and liquid hydrometeors, J. Geophys. Res., 89, 7170-7178, 1984.

Zawadzki, I., On radar-raingage comparison, J. Appl. Meteorol., 14, 1430-1436, 1975.

Zawadzki, I., Fractal structure and exponential decorrelation in rain, J. Geophys. Res., 92(D8), 9586-9590, 1987.

L. S. Chiu, General Sciences Corporation, 6100 Chevy Chase Drive, Laurel, MD 20707.

A. McConnell, Pixel Analysis, 9805 Gardiner Avenue, Silver Spring, MD 20902.

G. R. North, Climate System Research Program, Texas A&M University, College Station, TX 77843.

D. A. Short, Code 613, Goddard Space Flight Center, National Aeronautics and Space Administration, Greenbelt, MD 20771.

(Received November 28, 1988;
revised June 5, 1989;
accepted June 13, 1989.)